TOMOGRAPHY® RESEARCH ARTICLE

Tumor Sphericity Predicts Response in Neoadjuvant Chemotherapy for Invasive Breast Cancer

Wen Li[1], David C. Newitt[1], Bo La Yun[1,2], Ella F. Jones[1], Vignesh Arasu[1], Lisa J. Wilmes[1], Jessica Gibbs[1], Alex Anh-Tu Nguyen[1], Natsuko Onishi[1], John Kornak[3], Bonnie N. Joe[1], Laura J. Esserman[4], and Nola M. Hylton[1]

[1]Department of Radiology & Biomedical Imaging, University of California, San Francisco, San Francisco, CA; [2]Department of Radiology, Seoul National University Bundang Hospital, Seoul; Departments of [3]Epidemiology and Biostatistics; and [4]Surgery, University of California, San Francisco, San Francisco, CA

Corresponding Author:
Wen Li, PhD
UCSF Mt Zion Medical Center, 1600 Divisadero Street Box 1667,
San Francisco, CA 94115;
E-mail: wen.li@ucsf.edu

Key Words: Sphericity, magnetic resonance imaging, breast cancer, neoadjuvant therapy

Abbreviations: dynamic contrast-enhanced (DCE), neoadjuvant chemotherapy (NAC), sphericity (SPH), morphological pattern (MP), pathologic complete response (pCR), receiver operating characteristic (ROC), area under the curve (AUC), hormone receptor (HR), human epidermal growth factor receptor 2 (HER2), percent enhancement (PE), signal enhancement ratio (SER), surface area (SA), standard deviation (SD), confidence interval (CI)

ABSTRACT

This retrospective study examined magnetic resonance imaging (MRI)–derived tumor sphericity (SPH) as a quantitative measure of breast tumor morphology, and investigated the association between SPH and reader-assessed morphological pattern (MP). In addition, association of SPH with pathologic complete response was evaluated in patients enrolled in an adaptively randomized clinical trial designed to rapidly identify new agents for breast cancer. All patients underwent MRI examinations at multiple time points during the treatment. SPH values from pretreatment (T0) and early-treatment (T1) were investigated in this study. MP on T0 dynamic contrast-enhanced MRI was ranked from 1 to 5 in 220 patients. Mean SPH values decreased with the increased order of MP. SPH was higher in patients with pathologic complete response than in patients without (difference at T0: 0.04, 95% confidence interval [CI]: 0.02–0.05, $P < .001$; difference at T1: 0.03, 95% CI: 0.02–0.04, $P < .001$). The area under the receiver operating characteristic curve was estimated as 0.61 (95% CI, 0.57–0.65) at T0 and 0.58 (95% CI, 0.55–0.62) at T1. When the analysis was performed by cancer subtype defined by hormone receptor (HR) and human epidermal growth factor receptor 2 (HER2) status, highest area under the receiver operating characteristic curve were observed in HR−/HER2+: 0.67 (95% CI, 0.54–0.80) at T0, and 0.63 (95% CI, 0.51–0.76) at T1. Tumor SPH showed promise to quantify MRI MPs and as a biomarker for predicting treatment outcome at pre- or early-treatment time points.

INTRODUCTION

For women receiving neoadjuvant chemotherapy (NAC) for locally advanced breast cancer, achieving pathologic complete response (pCR) after the treatment conveys a likelihood for excellent outcome (1, 2). Dynamic contrast-enhanced magnetic resonance imaging (DCE-MRI) can be used to determine the extent of disease before, during, or after the NAC for breast cancer. The functional tumor volume calculated using contrast kinetic enhancement thresholds was found to be predictive of both pCR and event-free survival (3, 4). However, tumor volume has limited ability to assess tumor heterogeneity, which can be an important prognostic factor and associated with NAC response (5, 6). DCE-MRI can also be used to assess tumor heterogeneity, which may reflect the underlying tumor biology and potential treatment response (7–9). Previous studies have shown that distinct imaging patterns of tumor morphology predict response to NAC (10, 11). However, it is time-consuming and subject to reader variability to manually assess MRI morphological patterns (MPs).

With recent technology advances in medical imaging, artificial intelligence has demonstrated promises in cancer diagnosis, assessment of treatment response, and prediction of disease progression (12). In particular, radiomics has been used to extract quantitative imaging features such as tumor size, shape, texture, to study tumor characteristics in breast cancer (13). According to

© 2020 The Authors. Published by Grapho Publications, LLC This is an open access article under the CC BY-NC-ND license (http://creativecommons.org/licenses/by-nc-nd/4.0/).
ISSN 2379-1381 https://doi.org/10.18383/j.tom.2020.00016

the Image Biomarker Standardisation Initiative, sphericity (SPH) is one of the morphologic features to measure the shape of the tumor (14). Among all morphologic features, SPH may be used to differentiate tumor phenotypes, i.e. diffuse versus solid, independent from tumor size. Tumor SPH has been studied as a prognostic factor in oral (15) and lung cancers (16). To the best of our knowledge, no study of SPH has been reported in breast cancer based on MRIs. In this study, we propose to use an automatically derived SPH to quantify MRI MPs (17) by investigating and assessing the relationship between SPH and reader-assessed MP. We also investigated SPH as an imaging predictor for pCR, the endpoint of I-SPY 2 (Investigation of Serial Studies to Predict your Therapeutic Response with Imaging and Molecular Analysis 2) Trial.

METHODOLOGY

Patient Population

A cohort of 990 women from completed or graduated treatment arms of I-SPY 2 were considered in this study. Subjects gave written informed consent before enrollment and again after being randomized to treatment. All participating sites received approval from an institutional review board.

Treatment and Pathologic Outcome

Patients were treated for 12 weeks with 1 of 9 experimental drugs completed in I-SPY 2 by November 2016 or standard care, followed by administration anthracycline–cyclophosphamide (18, 19). pCR was used as the endpoint of the trial, defined as the absence of residual cancer in the breast and lymph nodes at the time of surgery. pCR was treated as a binary outcome in our analysis (1: pCR; 0: non-pCR).

Tumor Subtype

The primary tumor was categorized by hormone receptor (HR) and human epidermal growth factor receptor 2 (HER2) status (positive or absent/negative) at pretreatment, assessed from the core biopsy specimen by immunohistochemistry and Allred scores. The status of HR and HER2 define 4 breast tumor subtypes: HR+/HER2−, HR+/HER2+, HR−/HER2+, and HR−/HER2− (triple-negative).

Imaging Acquisition

MRI examinations were performed on 1.5 T or 3 T scanners across a variety of vendor platforms and institutions using a prospectively defined protocol. DCE-MRI was performed at multiple time points relative to treatment: before NAC (T0), after 3 weeks of NAC (T1), inter-regimen (T2), and presurgery (T3). Image acquisition parameters were as follows: repetition time = 4–10 milliseconds, minimum echo time ($\leq$4.8 milliseconds), flip angle = 10–20°, and field of view = 260–360 mm to achieve full bilateral coverage, acquisition matrix = 384–512 with in-plane resolution = $\leq$1.4 mm, and slice thickness = $\leq$2.5 mm. Three-dimensional fat-suppressed T1 images were acquired before and after injection of a gadolinium contrast agent. Postcontrast imaging was started simultaneously with injection. Phase duration was 80–100 seconds with a minimum of 8 minutes of imaging following injection. Gadolinium contrast agent was administrated intravenously at a dose of 0.1 mmol/kg body weight, and at a rate of 2 mL/s, followed by a 20-mL saline flush.

Morphological Pattern Assessment

Pretreatment DCE-MRI MP was visually assessed and graded by a radiologist without knowledge of clinical or histopathological findings using a ranking of 1–5 scale corresponding to the decreasing degree of tumor containment (see online supplemental Figure 1) definitions of MP were as follows: 1 = well-defined single mass, 2 = well-defined multilobulated mass, 3 = area enhancement with nodularity, 4 = area enhancement without nodularity, and 5 = septal spreading (11).

Sphericity

SPH was derived from the existing tumor mask created by the functional tumor volume calculation from DCE-MRI as previously described (20). In brief, the segmentation method involved calculating early percent enhancement (PE) and signal enhancement ratio (SER) maps using the following equations:

$$PE = 100 \times \frac{S_1 - S_0}{S_0}$$

$$SER = \frac{S_1 - S_0}{S_2 - S_0}$$

where S_0, S_1, and S_2 are intensity values from precontrast, 2.5 minutes, and 7.5 minutes after contrast, respectively. A tumor mask was created within a manually specified 3D region of interest (ROI) encompassing the enhancing lesion, using a PE $\geq$ 70% threshold. Voxels were further filtered with a precontrast intensity threshold of 60% of the maximum signal to remove suppressed fat and background noise voxels (3, 20). For the SPH calculation the tumor mask was further filtered using an SER $>$ 0.9 constraint to focus on plateau and washout characteristic enhancement. Surface area (SA) and volume were found for the resulting segmentation using a surface meshing analysis. SPH, defined as SA_0/SA_{tumor} where SA_{tumor} is the area of the tumor mask and SA_0 that of a sphere of the same volume, was calculated to quantify the similarity of the tumor morphology to a sphere (14). By the definition, with the similar volume, the scattered or multifoci tumor should have smaller SPH value than the single solid mass tumor. Processing was done using locally written software in IDL (Harris Geospatial, Broomfield, CO). SPH at T0 and T1 was calculated and tested for the prediction of pCR.

Statistical Analysis

Mean and standard deviation (SD) were calculated for SPH values within each MP and by cancer subtype. The comparison of means between all MPs was performed using the Tukey HSD (honestly significant difference) test. Wilcoxon rank sum test was used to estimate the difference in SPH variables between pCRs and non-pCRs. The predictive performance of SPH was assessed by the area under the receiver operating characteristic (ROC) curve (AUC). Statistical analyses were performed using R version 3.4.1 (R Foundation for Statistical Computing, Vienna, Austria). The pROC package was used to analyze ROC curves and calculate AUCs (21). Statistical significance was defined as $P < .05$.

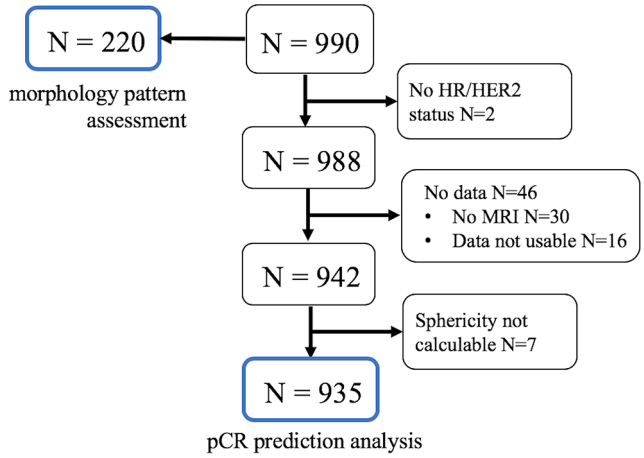


Figure 1. Flow diagram of patient cohorts included in this study. The numbers in blue frames indicate cohorts included in the analysis.

RESULTS

From the entire cohort of 990 patients, 2 subcohorts are referenced in the results of this study. Figure 1 shows patient selection in these cohorts. The first cohort consists of 220 patients with MP assessment at pretreatment, and SPH at T0 only was analyzed in this cohort. The mean and standard deviation of age in this cohort were 49 and 10 years, respectively. The second cohort consists of 935 patients with known pCR outcomes, SPH measured at T0 and T1, and HR (positive or negative)/HER2 receptor (positive or negative) status available. The mean and standard deviation of age in this cohort were 49 and 11 years, respectively. This cohort was used to analyze the association between SPH and pCR, in the full cohort and by HR/HER2 subtype. There was an overlap between the 2 cohorts (N = 210). Demographics of the first and the second cohorts are listed in Table 1. There was no statistically significant difference in age (P = .890), the frequency distribution of HR/HER2 status (P = .650), pCR outcome (P = .630), or SPH values at T0 (P = .890) between the analysis cohort and the cohort with MP assessment. Difference was found in menopausal status (P = .044). However, menopausal status was not considered in the analysis of this study.

Examples of MRI morphologic reading and SPH values of 2 different patients are shown in Figure 2. The 2 cases chosen illustrate differences in SPH (0.32 vs 0.13) resulting from tumor morphological differences for patients with very similar tumor volume (14.5 cc vs 14.0 cc). Figure 3 shows boxplots of SPH values vs MP for the full N = 220 cohort, and boxplots for individual HR/HER2 subcohorts are shown in the online supplemental Figure 2 (HR+/HER2−: N = 77; HR+/HER2+: N = 40; HR−/HER2+: N = 18; HR−/HER2−: N = 85). Mean and standard deviations are listed in online supplemental Table 1. Overall, the mean and median SPH values decreased with the increasing order of MP; that is, when going from single solid mass to more diffuse tumors. The 95% confidence intervals (CIs) for the differences in means between each pair of MPs are plotted in Figure 4. The numerical values are listed in online supplemental Table 2. Statistically significant differences were found between patterns 1, 2, and 3. Pattern 1 was also different from patterns 4 and 5 with P-values of 0.0017 and 0.001, respectively.

Table 1. Patient Characteristics of Included Cohort and Cohort with MRI Morphological Reading

	Cohort with Sphericity (n = 935)	Cohort with Morphologic Pattern (n = 220)	*P*-Value
Age[a]	49 ± 10	49 ± 11	.890
HR/HER2 Subtype			
HR+/HER2−	365 (39%)	77 (35.0%)	.650[b]
HR+/HER2+	148 (16%)	40 (18.2%)	
HR−/HER2+	80 (9%)	18 (8.2%)	
HR−/HER2−	342 (37%)	85 (38.6%)	
Menopausal Status			
Premenopausal	442 (47%)	105 (47.7%)	.044[b]
Perimenopausal	32 (3%)	1 (0.5%)	
Postmenopausal	271 (29%)	74 (33.6%)	
Not applicable	125 (13%)	22 (10%)	
Unknown	65 (7%)	18 (8.2%)	
SPH at T0[a]	0.22 ± 0.099	0.22 ± 0.095	.890
pCR Outcome			
0: non-pCR	625 (67%)	143 (65%)	.630[b]
1: pCR	310 (33%)	77 (35%)	

Abbreviations: HR, hormone receptor; HER2, human epidermal growth factor receptor 2; SP, sphericity.
[a] Values of age and SPH at T0 are mean ± standard deviation.
[b] Estimated by Fisher exact test.

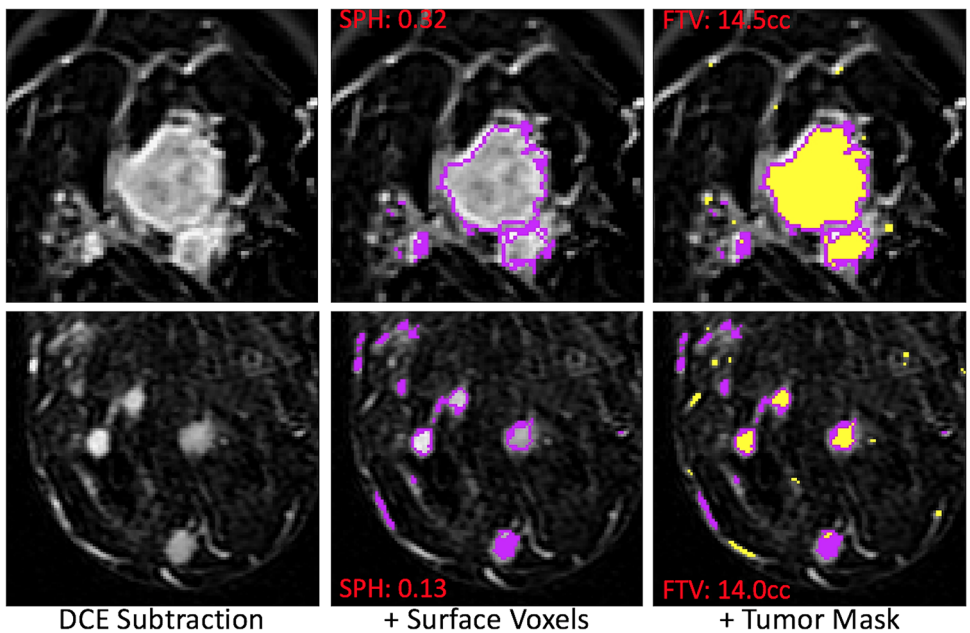


Figure 2. Example magnetic resonance (MR) images of patients with different morphologic readings. Representative slices of axial magnetic resonance imaging (MRI) were shown from 2 patients. The morphologic readings were 1 and 3 for the top and bottom row, respectively. The sphericity (SPH) values are 0.32 for the top and 0.13 for the bottom. However, the tumor volumes are close (14.5 cc for the top and 14 cc for the bottom).

In the cohort of 935 patients, 310 (33%) achieved pCR after NAC and 625 (67%) did not (non-pCRs). pCR rate varied among HR/HER2 subtypes. They were 18% (66 out of 365) in HR+/HER2−, 40% (59 out of 148) in HR+/HER2+, 61% (49 out of 80) in HR−/HER2+, and 41% (140 out of 342) in HR−/HER2− (triple-negative). Table 2 shows differences between pCR and non-pCR for median SPH at T0 and T1. The overall observation is that SPH is higher in patients who achieved pCR than in those with non-pCRs. The median difference in SPH was found to be statistically significant in the full cohort ($P = .001$) and in HR− (HER2+/−) cancer subtypes ($P = .011$ and $P = .047$ at T0 and T1 for HR−/HER2+; $P = .001$ at both time points for the triple-negative subtype. The difference in HR+/HER2− was statistically significant at T0 ($P = .008$) but not at T1 ($P = .054$). No statistical difference was found in HR+/HER2+ at either time point ($P = .120$ at T0, $P = .550$ at T1).

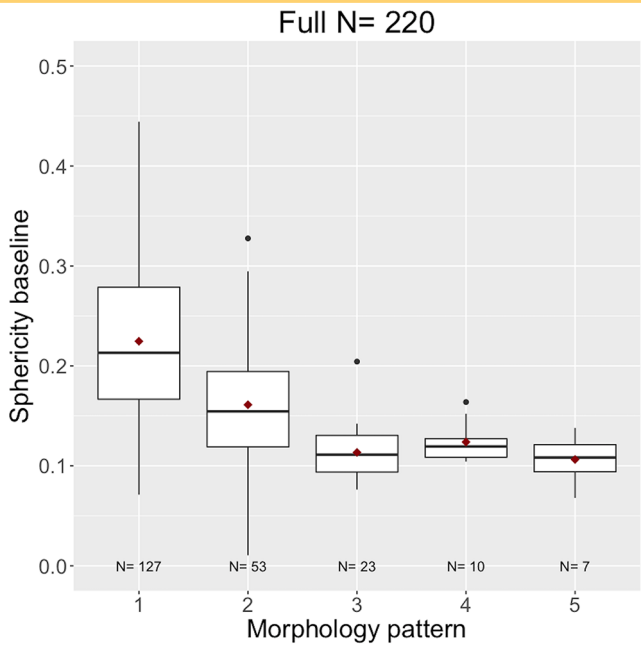


Figure 3. Boxplots of SPH values versus morphological patterns (MPs). The *x*-axis is patterns 1 to 5, while the *y*-axis is the SPH value at baseline. The line in each boxplot represents the median, and the red dot represents the mean.

AUCs of using SPH to predict pCR in the full cohort and in individual subtypes are listed in Table 3, and corresponding ROC curves are shown in Figure 5. Overall, AUC was lower after the treatment started (at T1) than before treatment (at T0). In the full cohort, SPH at T0 and T1 was predictive of pCR with estimated AUCs of 0.61 and 0.58, respectively. Among the subtypes, the highest AUCs were observed in HR−/HER2+ with estimated values of 0.67 at T0 and 0.63 at T1. The lowest AUCs were observed in HR+/HER2+ with estimated values of 0.58 at T0 and 0.53 at T1. CIs showed that AUCs estimated for this subtype at both time points and for HR+/HER2− at T1 were not above 0.5 (nondiscriminatory test) with statistical significance.

DISCUSSION

In this study, we investigated using tumor SPH to quantify MRI MPs and to predict pCR. Previously it was noted that different tumor phenotypes in MRI responded differently to NAC treatments (10), and further evidence of this dependence was shown in a study using I-SPY 1/ACRIN 6657 data (11). In this current study, we tested the usage of the quantitatively measured SPH, a morphological measure derivable from the tumor mask generated

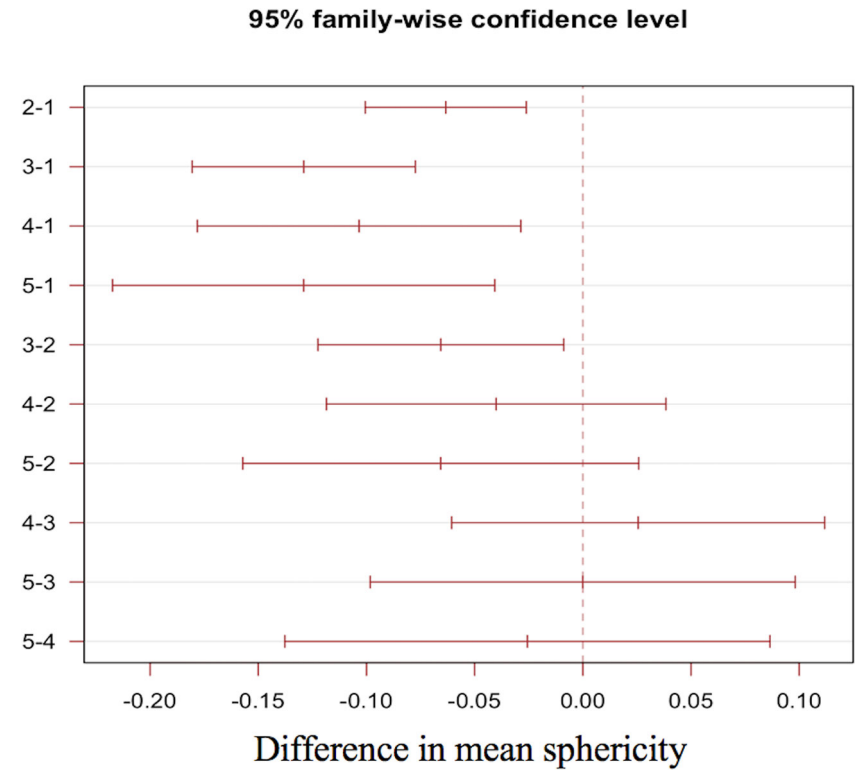


Figure 4. Pairwise 95% confidence intervals (CIs) of differences in mean SPHs between MPs. The *x*-axis is the differences in mean SPHs, and the y-axis is the pattern pair. At the 95% CI level, horizontal lines staying at one side of the vertical line at zero were statistically significant.

from DCE-MRI tumor volume calculation, in distinguishing tumor phenotypes by comparing it to the MRI MP assessed by a radiologist. Mathematically, SPH is a measure of how closely the shape of an object is to a perfect sphere. Theoretical SPH values range from just >0 for a very diffuse object to 1 for a perfect sphere, but this range will be reduced for finite digitized 3D images such as MRI. Solid tumors with roughly spherical shapes have high SPH values, while scattered or multifoci tumors have low SPH values. Our results showed that SPH values for tumors classified with MPs 1, 2, and 3 in MRI decreased significantly with respect to the order, but the differences between MPs 3, 4, and 5 were not as obvious. A similar trend was observed in the

Table 2. SPH Values for Patients with pCR versus Non-pCR

	N	pCR Rate (N)[a]	pCR	Non-pCR[a]	Difference[b]	*P*-Value
T0						
Full	935	33% (309)	0.23 (0.16, 0.30)	0.18 (0.13, 0.26)	0.04 (0.02, 0.05)	**.001**
HR+/HER2−	365	18% (66)	0.22 (0.16, 0.31)	0.20 (0.14, 0.26)	0.04 (0.01, 0.06)	**.008**
HR+/HER2+	148	40% (59)	0.24 (0.16, 0.33)	0.19 (0.14, 0.29)	0.03 (−0.007, 0.06)	.120
HR−/HER2+	80	61% (49)	0.24 (0.17, 0.28)	0.16 (0.10, 0.26)	0.06 (0.01, 0.10)	**.011**
HR−/HER2− (triple-negative)	342	41% (140)	0.23 (0.17, 0.29)	0.18 (0.13, 0.24)	0.04 (0.02, 0.06)	**.001**
T1						
Full	935	33% (309)	0.22 (0.16, 0.32)	0.20 (0.14, 0.27)	0.03 (0.02, 0.04)	**.001**
HR+/HER2−	365	18% (66)	0.25 (0.15, 0.33)	0.21 (0.14, 0.27)	0.03 (−0.0005, 0.06)	.054
HR+/HER2+	148	40% (59)	0.21 (0.16, 0.32)	0.20 (0.15, 0.31)	0.01 (−0.03, 0.04)	.550
HR−/HER2+	80	61% (49)	0.23 (0.16, 0.30)	0.18 (0.12, 0.25)	0.05 (0.0007, 0.09)	**.047**
HR−/HER2− (triple-negative)	342	41% (140)	0.23 (0.16, 0.32)	0.19 (0.13, 0.25)	0.04 (0.02, 0.06)	**.001**

Abbreviations: AUC, area under the curve; pCR, pathologic complete response; HR, hormone receptor; HER2, human epidermal growth factor receptor 2.
[a] Values in pCR and Non-pCR columns are given as median (interquartile range).
[b] Values in the Difference column are given as the median difference and 95% CIs in parenthesis. *P*-values < .05 are in bold.

Table 3. AUCs of SPH in the Prediction of pCR at Different Treatment Time Points

Cohort	N	pCR Rate	T0	T1
Full	935	33%	0.61 (0.57, 0.65)	0.58 (0.55, 0.62)
HR+/HER2−	365	18%	0.61 (0.53, 0.68)	0.58 (0.49, 0.66)
HR+/HER2+	148	40%	0.58 (0.48, 0.67)	0.53 (0.43, 0.62)
HR−/HER2+	80	61%	0.67 (0.54, 0.80)	0.63 (0.51, 0.76)
HR−/HER2−	342	41%	0.64 (0.58, 0.70)	0.62 (0.56, 0.68)

Abbreviations: AUC, area under the curve; pCR, pathologic complete response; HR, hormone receptor; HER2, human epidermal growth factor receptor 2.

HR/HER2 subtype subgroup. However, compared with the manual MP reading, SPH is an automatically calculated measure (aside from the manual selection of a bounding volume of interest box). It is highly reproducible. The lack of differentiation between the higher-order patterns may be partially due to the limit number of cases. However, the description of 5 MRI MPs can be ambiguous and difficult to reproduce, particularly among patterns 3, 4, and 5 (11). So the ability of any quantitative morphological metric to differentiate between these higher-order, more diffuse tumors may be severely limited.

We also tested SPH as a quantitative predictor for treatment response in patients who received NAC, and results showed that SPH at pretreatment appears to be higher in patients who had pCR than in patients who did not have pCR. The same trend was observed at T1, 3 weeks after NAC initiated. This result confirms previous finding that there is a higher chance of pCR for more circumscribed lesions (10, 11). AUCs also showed that SPH can differentiate pCR versus non-pCR at pre- or early-treatment time points. This finding is helpful in making clinical decisions, especially for HR+/HER2− cancer subtype, which has the lowest pCR rate among all subtypes for patients who underwent NAC. Alternative therapy could be used on patients who are not going to benefit from NAC. The fact that AUCs decrease from pretreatment to early-treatment time point showed SPH is the most predictive at pretreatment of NAC. Compared with other imaging technologies (mainly mammography and ultrasonography), MRI showed the highest accuracy in predicting pCR (22). However, very few studies report MRI features measured at pretreatment being predictive (23). Radiomics is a rising research tool in cancer imaging, which extracts a large number of imaging features and leverages machine learning algorithms to reveal underlying biology heterogeneity and predict treatment response. A recent published multicenter study showed that radiomics can be a potential tool to predict pCR for patients with breast cancer who underwent NAC (24). The current study focused on one feature that can be automatically calculated from DCE-MRI as a byproduct of functional tumor volume, an established biomarker having been used in NAC clinical trials for decades (3, 25).

Our study has several limitations. First, the radiologist read a subset of the full cohort, which may not represent the entire population. However, composition of the two cohorts was similar in terms of receptor subtype and pCR rates. Second, only one radiologist performed the reading, which has subjective components and will result in inter-reader

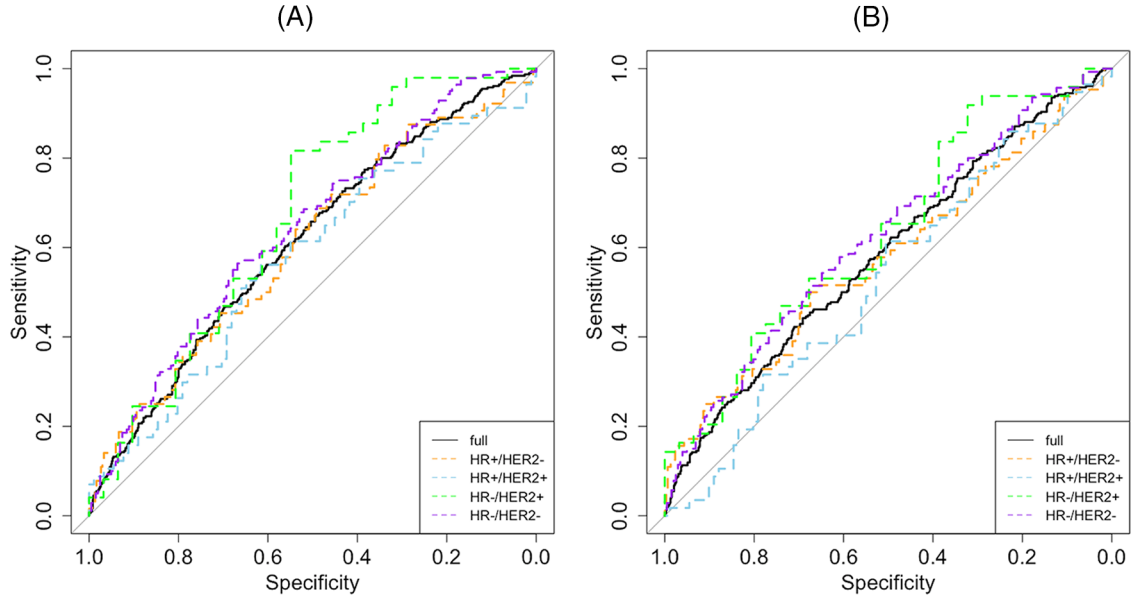


Figure 5. Receiver operating characteristic curves of SPH in predicting pathologic complete response. SPH measured at pretreatment (A) and SPH measured at early-treatment time point (B). The diagonal line in gray represents a non-discriminatory test (area under the curve = 0.5).

variability that could affect the relation between SPH and phenotype. Third, SPH measurement requires a minimum number of voxels in the tumor mask. When tumor dissolves or shrinks to minimum residual, the remaining tumor may not contain enough number of voxels and thus SPH is not calculable in these cases. With our current processing, this could severely bias any analysis due to the resulting exclusion of patients showing rapid treatment effects, and thus SPH may be best applied to the index disease, and not as tumor responds.

In conclusion, this study showed the ability of an automated SPH measure to capture breast tumor phenotype in DCE-MRI. SPH at pretreatment alone predicted pCR. In future studies, other radiomics features that can be used as quantitative measures for tumor phenotypes will be explored. Furthermore, the possible combination of different selected features may also improve the prediction of treatment response.

Supplemental Figure

Supplemental Figure 1: https://doi.org/10.18383/j.tom.2020.00016.sup.01

Supplemental Figure 2: https://doi.org/10.18383/j.tom.2020.00016.sup.02

Supplemental Table 1: https://doi.org/10.18383/j.tom.2020.00016.sup.03

Supplemental Table 2: https://doi.org/10.18383/j.tom.2020.00016.sup.04

ACKNOWLEDGMENTS

This work was supported in part by NIH grants: R01 CA132870, U01 CA225427, and P01 CA210961.

Conflict of Interest: None reported.

Disclosures: No disclosures to report.

REFERENCES

1. Kong X, Moran MS, Zhang N, Haffty B, Yang Q. Meta-analysis confirms achieving pathological complete response after neoadjuvant chemotherapy predicts favourable prognosis for breast cancer patients. Eur J Cancer. 2011;47:2084–2090.
2. von Minckwitz G, Untch M, Blohmer J-U, Costa SD, Eidtmann H, Fasching PA, Gerber B, Eiermann W, Hilfrich J, Huober J, Jackisch C, Kaufmann M, Konecny GE, Denkert C, Nekljudova V, Mehta K, Loibl S. Definition and impact of pathologic complete response on prognosis after neoadjuvant chemotherapy in various intrinsic breast cancer subtypes. J Clin Oncol. 2012;30:1796–1804.
3. Hylton NM, Blume JD, Bernreuter WK, Pisano ED, Rosen MA, Morris EA, Weatherall PT, Lehman CD, Newstead GM, Polin S, Marques HS, Esserman LJ, Schnall MD. Locally advanced breast cancer: MR imaging for prediction of response to neoadjuvant chemotherapy–results from ACRIN 6657/I-SPY TRIAL. Radiology. 2012;263:663–672.
4. Hylton NM, Gatsonis CA, Rosen MA, Lehman CD, Newitt DC, Partridge SC, Bernreuter WK, Pisano ED, Morris EA, Weatherall PT, Polin SM, Newstead GM, Marques HS, Esserman LJ, Schnall MD. Neoadjuvant chemotherapy for breast cancer: functional tumor volume by MR imaging predicts recurrence-free survival-results from the ACRIN 6657/CALGB 150007 I-SPY 1 TRIAL. Radiology. 2016;279:44–55.
5. Junttila MR, de Sauvage FJ. Influence of tumour micro-environment heterogeneity on therapeutic response. Nature. 2013;501:346–354.
6. Perou CM, Sørlie T, Eisen MB, van de Rijn M, Jeffrey SS, Rees CA, Pollack JR, Ross DT, Johnsen H, Akslen LA, Fluge Ø, Pergamenschikov A, Williams C, Zhu SX, Lønning PE, Børresen-Dale A-L, Brown PO, Botstein D. Molecular portraits of human breast tumours. Nature. 2000;406:747–752.
7. Fowler AM, Mankoff DA, Joe BN. Imaging neoadjuvant therapy response in breast cancer. Radiology. 2017;285:358–375.
8. Gillies RJ, Raghunand N, Karczmar GS, Bhujwalla ZM. MRI of the tumor microenvironment. J Magn Reson Imaging. 2002;16:430–450.
9. Davnall F, Yip CSP, Ljungqvist G, Selmi M, Ng F, Sanghera B, Ganeshan B, Miles KA, Cook GJ, Goh V. Assessment of tumor heterogeneity: an emerging imaging tool for clinical practice? Insights Imaging. 2012;3:573–589.
10. Esserman L, Kaplan E, Partridge S, Tripathy D, Rugo H, Park J, Hwang S, Kuerer H, Sudilovsky D, Lu Y, Hylton N. MRI phenotype is associated with response to doxorubicin and cyclophosphamide neoadjuvant chemotherapy in stage III breast cancer. Ann Surg Oncol. 2001;8:549–559.
11. Mukhtar RA, Yau C, Rosen M, Tandon VJ, Hylton N, Esserman LJ. Clinically meaningful tumor reduction rates vary by prechemotherapy MRI phenotype and tumor subtype in the I-SPY 1 TRIAL (CALGB 150007/150012; ACRIN 6657). Ann Surg Oncol. 2013;20:3823–3830.
12. Bi WL, Hosny A, Schabath MB, Giger ML, Birkbak NJ, Mehrtash A, Allison T, Arnaout O, Abbosh C, Dunn IF, Mak RH, Tamimi RM, Tempany CM, Swanton C, Hoffmann U, Schwartz LH, Gillies RJ, Huang RY, Aerts HJWL. Artificial intelligence in cancer imaging: clinical challenges and applications. CA Cancer J Clin. 2019;69.
13. Tagliafico AS, Piana M, Schenone D, Lai R, Massone AM, Houssami N. Overview of radiomics in breast cancer diagnosis and prognostication. Breast. 2020;49:74–80.
14. Zwanenburg A, Leger S, Vallieres M, Lock S. Image biomarker standardisation initiative. 2019.
15. Tarsitano A, Ricotta F, Cercenelli L, Bortolani B, Battaglia S, Lucchi E, Marchetti C, Marcelli E. Pretreatment tumor volume and tumor sphericity as prognostic factors in patients with oral cavity squamous cell carcinoma. J Craniomaxillofac Surg. 2019;47:510–515.
16. Davey A, van Herk M, Faivre-Finn C, Mistry H, McWilliam A. Is tumour sphericity an important prognostic factor in patients with lung cancer? Radiother Oncol. 2020;143:73–80.
17. Newitt DC, Li W, B La Y, Esserman LJ. I-SPY 2 Consortium, Hylton NM. Tumor sphericity as a predictor of response in patients undergoing neoadjuvant chemotherapy treatment for invasive breast cancer. In: ISMRM Annual Meeting. Montreal, Canada; 2019.
18. Park JW, Liu MC, Yee D, Yau C, van 't Veer LJ, Symmans WF, Paoloni M, Perlmutter J, Hylton NM, Hogarth M, DeMichele A, Buxton MB, Chien AJ, Wallace AM, Boughey JC, Haddad TC, Chui SY, Kemmer KA, Kaplan HG, Isaacs C, Nanda R, Tripathy D, Albain KS, Edmiston KK, Elias AD, Northfelt DW, Pusztai L, Moulder SL, Lang JE, Viscusi RK, Euhus DM, Haley BB, Khan QJ, Wood WC, Melisko M, Schwab R, Helsten T, Lyandres J, Davis SE, Hirst GL, Sanil A, Esserman LJ, Berry DA. Adaptive randomization of Neratinib in early breast cancer. N Engl J Med. 2016;375:11–22.
19. Rugo HS, Olopade OI, DeMichele A, Yau C, van 't Veer LJ, Buxton MB, Hogarth M, Hylton NM, Paoloni M, Perlmutter J, Symmans WF, Yee D, Chien AJ, Wallace AM, Kaplan HG, Boughey JC, Haddad TC, Albain KS, Liu MC, Isaacs C, Khan QJ, Lang JE, Viscusi RK, Pusztai L, Moulder SL, Chui SY, Kemmer KA, Elias AD, Edmiston KK, Euhus DM, Haley BB, Nanda R, Northfelt DW, Tripathy D, Wood WC, Ewing C, Schwab R, Lyandres J, Davis SE, Hirst GL, Sanil A, Berry DA, Esserman LJ. Adaptive randomization of Veliparib-Carboplatin treatment in breast cancer. N Engl J Med. 2016;375:23–34.
20. Newitt DC, Aliu SO, Witcomb N, Sela G, Kornak J, Esserman L, Hylton NM. Real-time measurement of functional tumor volume by MRI to assess treatment response in breast cancer neoadjuvant clinical trials: validation of the Aegis SER software platform. Transl Oncol. 2014;7:94–100.
21. Robin X, Turck N, Hainard A, Tiberti N, Lisacek F, Sanchez J-C, Müller M. pROC: an open-source package for R and S+ to analyze and compare ROC curves. BMC Bioinformatics. 2011;12:77.
22. Yuan Y, Chen X-S, Liu S-Y, Shen K-W. Accuracy of MRI in prediction of pathologic complete remission in breast cancer after preoperative therapy: a meta-analysis. AJR Am J Roentgenol. 2010;195:260–268.
23. Prevos R, Smidt ML, Tjan-Heijnen VCG, van Goethem M, Beets-Tan RG, Wildberger JE, Lobbes MBI. Pre-treatment differences and early response monitoring of neoadjuvant chemotherapy in breast cancer patients using magnetic resonance imaging: a systematic review. Eur Radiol. 2012;22:2607–2616.
24. Liu Z, Li Z, Qu J, Zhang R, Zhou X, Li L, Sun K, Tang Z, Jiang H, Li H, Xiong Q, Ding Y, Zhao X, Wang K, Liu Z, Tian J. Radiomics of multiparametric MRI for pretreatment prediction of pathologic complete response to neoadjuvant chemotherapy in breast cancer: a multicenter study. Clin Cancer Res. 2019;25:3538–3547.
25. Esserman L, Hylton N, Asare S, Yau C, Yee D, DeMichele A, Perlmutter J, Symmans F, van't Veer L, Matthews J, Donald AB, Barker A. I-SPY2: Unlocking the Potential of the Platform Trial. In: Antonijevic Z, Beckman RA, editors. Platform Trial Designs in Drug Development: Umbrella Trials and Basket Trials. Chapman and Hall/CRC; 2018. p. 3–22.